Vol 11 No 3, March 2002
1009-1963/2002/11(03)/0226-07

Chinese Physics

© 2002 Chin. Phys. Soc.
and IOP Publishing Ltd

Numerical simulation of dispersion generated by a 180° turn in a microchannel*

Yao Zhao-Hui(姚朝晖)[a)b)†], G. L. Yoder[b)], C. T. Culbertson[c)], and J. M. Ramsey[c)]

[a)] *Department of Engineering Mechanics, Tsinghua University, Beijing* 100084, *China*

[b)] *Engineering Technology Division, Oak Ridge National Laboratory, P.O. Box* 2009, *Oak Ridge, Tennessee* 37831-8045, *USA*

[c)] *Chemical and Analytical Sciences Division, Oak Ridge National Laboratory P.O. Box* 2008, *Oak Ridge, Tennessee* 37831-6142, *USA*

(Received 11 July 2001; revised manuscript received 18 November 2001)

A numerical scheme is developed to simulate electro-osmotic flow and mass transport in a microchannel which includes a 180° turn. The model has been used to predict the behaviour of electro-osmotically driven flows. The detailed structure of the flow field in a microchannel in combination with species mass diffusion can explain the concentration dispersion introduced by a 180° turn. The results of our simulations agree both qualitatively and quantitatively with experimental observation. It is demonstrated that an improved electro-osmotic force model could simulate the electrokinetically driven flow well without making detailed calculations of the electric charge density distribution within the electrical double layer. Additionally, because this model applies forces to the liquid as opposed to imposing local velocities, it should also be appropriate for use where pressure gradients exist in the flow field.

Keywords: surface chemistry, molecular diffusion, numerical simulation, microchannel
PACC: 0540, 4765, 5190

1. Introduction

Nanodevices and microdevices of fluids have been widely used in electrically driven separation techniques, such as capillary electrophoresis (CE), synchronized cyclic electrophoresis (SCE) and micellar electrokinetic chromatography (MEKC).[1−4] Because the advantages of combining sample processing and analysis in a single device are numerous, these separation techniques are being integrated with other physical manipulations and chemical treatments on microchip devices. Increasing the level of integration, however, results in a more complex channel structure with a greater number of channels and interconnections. This integration often requires several turns to be introduced into the channels.[1,5] The introduction of turns adds a geometric contribution to analyte dispersion as both the migration distance and electric field strength vary laterally across the width of the channel in the turns.[6,7]

Computer simulation is expected to be useful in the basic research of electrokinetic sample transport and dispersion phenomena in the channel manifold.[8−11] It can also be used to optimize the microchip channel geometry and operating parameters. Some models have been proposed to account for the excess dispersion.[12,13] All these models, however, describe the source of dispersion introduced by turns with analytical methods. These analytical methods depend on assumptions and experimental results to develop a general description of the process. Mathematical models of electro-osmotic transport have been developed to describe this phenomenon. However, they cannot describe the dispersion process in detail. Most models are limited to one-dimensional analysis. However, there are a few reports which numerically solve two-dimensional (2D) and three-dimensional (3D) problems in straight rectangular channels.[14−16] These simulations usually assume that the process is in steady state.

In this paper, a numerical simulation of analyte dispersion in two microchip channel geometries is performed and compared to experimental results. The results are presented from both static dispersion (no net fluid motion) and dispersion generated by a 180° turn with electro-osmotically induced fluid motion. The detailed structure of the flow field explains the change in geometric shape of the analyte as it traverses the 180° turn, while the species transport process clearly explains the broadening of the analyte mass distribution.

*Project supported by the National Natural Science Foundation of China (Grant No 19902009).

†Corresponding author: yaozh@tsinghua.edu.cn; Tel. 010-62785560

2. Description of geometry and solution

2.1. Static diffusion

The initial calculations were performed to examine the static diffusion of rhodamine B analyte in a buffer solution of 50/50 (v/v) 20mM sodium tetraborate/methanol in a straight channel on a microchip. The microchip was fabricated using standard photolithography, wet chemical etching and thermal bonding techniques as previously described.[7] The analysis channel on this chip was 9μm in depth and 89μm in width at half-depth. To measure the diffusion coefficient, a plug of rhodamine B was injected into the analysis channel and electromigrated to the centre of the detection window. At this point the electric potentials were removed from the microchip. Images of the analysis channel containing the analyte were then taken every five seconds for two minutes, using a laser-induced fluorescence technique.[17] Concentration profiles of the analyte were obtained by summing the signal across the width of the channel. The analyte concentration as a function of peak variance was then plotted.

2.2. Diffusion in a 180° turn

The analysis of 180° turn dispersion presented in this paper is compared to an experiment where a discrete volume of rhodamine B is injected into a channel which includes a 180° turn. The microchip containing this channel was fabricated in a manner similar to that used to fabricate the straight channel chip described above, and the experimental imaging technique was the same. As the rhodamine B volume traverses the channel, dispersion of the analyte occurs due to molecular diffusion and the differences in migration length and field strength in the turn.

The geometry of the device is shown in Fig.1. The channel is 9μm in depth and 89μm in width at half-depth. The length from the inlet to the outlet of the 180° turn is 6.15 mm. The buffer solution used in this experiment is 50/50 20 mM sodium tatraborate/methanol, and the analyte is rhodamine B. Fluid motion is driven by electro-osmosis under an applied external electric field.

The objective of the present work is to predict the dispersion behaviour of the analyte under static conditions and on passing through the 180° turn.

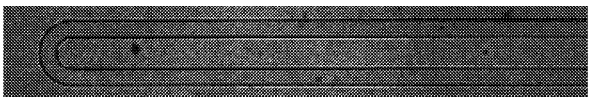


Fig.1. Image of the microchannel with a 180° turn used in the experiment.

3. Mathematical model

For the 180° turn experiment, the average experimental fluid velocity in the microchannel is very small (∼0.0008m/s) and the flow is laminar. The Lewis number $\left(\frac{\rho D}{k/C_{\mathrm{p}}}\right)$ is much less than 1, so that the transport of enthalpy due to species diffusion can be neglected. We have further assumed that the physical properties of the solution remain constant during the species transport process, and that ohmic heating of the fluid due to the imposed potential field is negligible. Additionally, it is assumed that the electrical double layer is small compared to the channel dimensions, and that the analyte concentration is sufficiently low so that the electric conductivity is not spatially dependent.

Making the above assumptions, the basic equations describing the flow and mass transport are as follows.

Continuity equation:

$$\nabla \cdot \boldsymbol{V} = 0. \tag{1}$$

Momentum equation:

$$\rho \frac{\partial \boldsymbol{V}}{\partial t} + \rho(\boldsymbol{V} \cdot \nabla)\boldsymbol{V} = -\nabla p + \mu \nabla^2 \boldsymbol{V} + \boldsymbol{F}_{\mathrm{e}}. \tag{2}$$

Here $\boldsymbol{V}$ is the velocity, ρ is the density, p is the pressure, and μ is the viscosity. $\boldsymbol{F}_{\mathrm{e}}$ is electric force, which can be given by the product of the electric charge density ρ_{e} times the electric field intensity $\boldsymbol{E}$

$$\boldsymbol{F}_{\mathrm{e}} = \rho_{\mathrm{e}} \boldsymbol{E}. \tag{3}$$

The electric field is related to the electric potential Φ by

$$\boldsymbol{E} = -\nabla \Phi, \tag{4}$$

while the electric potential Φ is governed by Poisson's equation

$$\nabla^2 \Phi = -\frac{\rho_{\mathrm{e}}}{\varepsilon_0 \varepsilon}, \tag{5}$$

where ε is the dielectric constant of the solvent, and ε_0 is the dielectric permittivity of the vacuum.

The connection between the equations of motion and the calculation of the electric field potential enters through the body force term $\boldsymbol{F}_{\mathrm{e}}$ in the momentum

equation (2). The relationship between the body force $\boldsymbol{F}_{\mathrm{e}}$ and the electric field potential Φ can, therefore, be obtained by making use of Poisson's equation which gives the relationship between the electric field potential and the field charge density.

However, Eq.(5) can be simplified to the Laplace equation in the absence of free charges

$$\nabla^2 \Phi = 0. \tag{6}$$

Because the fluids under consideration have zero net charge, the solution of the Laplace equation can be used to solve the far field potentials.

The solid surface being investigated (glass) has an electrostatic charge that can be used to promote electrokinetic flow. The charged surface of the glass, when in contact with the buffer solution of sodium tetraborate/methanol, attracts ions in the buffer solution, forming a layer of oppositely charged ions on the surface. The surface charge repels like charged ions from the surface. The distribution of these charges perpendicular to the glass surface forms a very thin layer (of the order of a few nanometres) commonly called the electrical double layer (EDL). Beyond the layer, in the bulk of the buffer, the net charge is zero with equal numbers of positive and negative charges. The existence of the charge distribution in the double layer allows flow to be driven by applying an electric field (electro-osmosis). In our calculations, we have not tried to resolve the double layer since we are only interested in the diffusion characteristics in the main portion of the flow. We have, therefore, applied the electro-osmotically induced force only to the cells next to the wall. In our calculations, the grid size is of the order of 10^{-7}m, so that this assumption is reasonable. Models for electrophoritic transport have been developed previously,[18] while electro-osmotic flow profiles have been theoretically calculated for simple geometries, such as narrow capillary slits[19] and cylindrical capillaries.[20] For complicated geometries,[15] it has been assumed that the liquid slips along the wall with a velocity $\boldsymbol{V} = \mu_{\mathrm{eo}}\boldsymbol{E}$, where μ_{eo} is the electro-osmotic mobility.

In chemical physics,[21] the electro-osmotic mobility μ_{eo} of a particle is defined as

$$\mu_{\mathrm{eo}} = \frac{\boldsymbol{V}}{\boldsymbol{E}}.$$

The calculation of a particle's mobility assumes that the forces acting on the particle are only the electric and viscous forces, which have the same value but opposite directions

$$\boldsymbol{F}_{\mathrm{vis}} = -\boldsymbol{F}_{\mathrm{e}}.$$

For Stokes flow

$$-f\boldsymbol{V} = -q\boldsymbol{E},$$

$$\mu_{\mathrm{eo}} = \frac{\boldsymbol{V}}{\boldsymbol{E}} = \frac{q}{f}$$

where q is the charge of the particle and f is a factor which includes the particle drag coefficient. Similarly, for flow in a straight channel, if there is no pressure drop, the channel buffer velocity can be determined using $\boldsymbol{V} = \mu_{\mathrm{eo}}\boldsymbol{E}$, where μ_{eo} is usually determined empirically in straight channel geometries. This formulation has previously been used for numerical analysis of two-dimensional electro-osmotic flows by patching this velocity on the wall boundary.[15] However, for flow that is driven by both a potential gradient and a pressure gradient, the forces acting on the particle are the electric force, the viscous force and the pressure force. Evidently, it is incorrect to calculate the fluid velocity using $\boldsymbol{V} = \mu_{\mathrm{eo}}\boldsymbol{E}$ when a pressure gradient is present. As an example, Fig.2 shows that the pressure gradient near the intersection of a turn and a straight channel is not zero, even though the flow is driven only by an external electric potential. It is, therefore, not appropriate to patch the velocity on the cells next to the wall using $\boldsymbol{V} = \mu_{\mathrm{eo}}\boldsymbol{E}$. However, if the applied potential gradient is fixed, the electrically-induced force remains constant regardless of the existence of a pressure gradient. To incorporate this physical behaviour into the model we have chosen to patch the electrically-induced force on the cell near the wall. In this cell, the viscous force in the x-direction, $\boldsymbol{F}_{\mathrm{vis},x}$, can be obtained by the product of the wall shear stress τ_w times the shear area A_w, i.e.

$$\boldsymbol{F}_{\mathrm{ex}} = \boldsymbol{F}_{\mathrm{vis},x} = \tau_w A_w = \mu\frac{\partial u}{\partial y}A_w, \tag{7}$$

where μ is the fluid viscosity, and $\partial u/\partial y$ is the velocity gradient at the wall (here assumed to be linear). Since the mobility is determined in the absence of a pressure gradient, and if we assume that the fluid velocity in the x-direction at the outer boundary of the cell can be calculated using $u = u_{\mathrm{eo}}E_x$, the field-induced force in the x-direction on the near wall cell can be expressed by

$$\boldsymbol{F}_{\mathrm{ex}} = \mu\frac{\mu_{\mathrm{eo}}E_x}{\Delta y}A_w. \tag{8}$$

The species transport equation can be expressed as

$$\frac{\partial C}{\partial t} + (\boldsymbol{V} \cdot \nabla)C = D\nabla^2 C, \tag{9}$$

where C is the sample concentration, and D is the molecular diffusion coefficient.

Equations (1), (2), (4), (5), (7) and (9) are used to calculate the flow and mass transport in electro-osmotically driven flows in a microchannel.

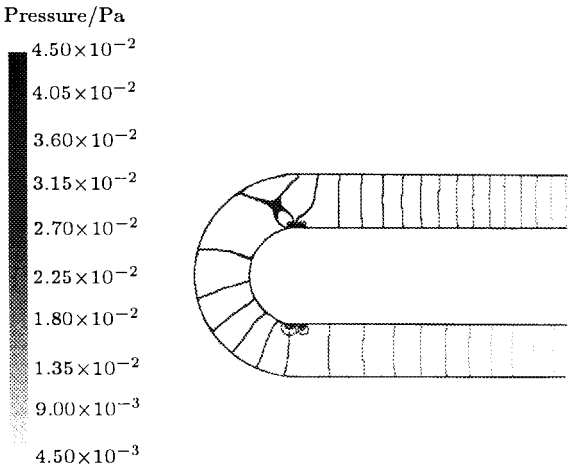


Fig.2. Contours of pressure.

Additionally, we need to specify the boundary conditions for the problem. For the electric potential due to the applied external electric field Φ, we impose a zero gradient condition at the channel wall, and impose constant potentials on the inlet and outlet. For the flow field, we have assumed pressure boundary conditions at both inlet and outlet with a zero pressure drop specified along the channel. A no-slip condition is used on the wall. For the species transport problem, zero flux is assumed on all solid boundaries.

4. Numerical simulation and results

Two-dimensional calculations of flow and species transport in the microchannel with a 180° turn were performed using the geometry as well as the boundary and initial conditions noted above.

4.1. Static diffusion

The simulation of the static diffusion problem, as discussed in section 2 above, started with the experimental distribution of rhodamine B at time t=0. The concentration profile was assumed to extend across the full width and depth of the channel. The time-dependent solution of the diffusion equations was then initiated. The results of the calculations are shown in Fig.3. In order to compare the calculations with the experimental results, the peak fluorescence level at t=0 of the experiment was normalized to a value of one. Figure 3 compares experimental and numerical results at three different times during the diffusion process. The data are indicated with solid symbols, while the calculated results are presented as solid lines. In addition, Table 1 shows a comparison of calculated and experimentally determined peak values at various times. As indicated by both Fig.3 and Table 1, the calculated results agree quite well with experimental data, giving some confidence that the numerical calculations capture the time-dependent species diffusion adequately.

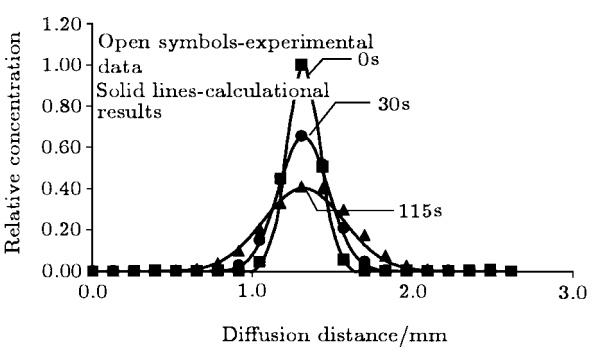


Fig.3. Comparison of experimental and calculated analyte diffusion in a stagnant channel.

Table 1. Peak concentration as a function of time.

Time/s	Relative concentration (experimental)	Relative concentration (calculated)	Error/%
0	1.0	1.0	0
30	0.657	0.647	−3.2
60	0.529	0.517	−2.3
90	0.453	0.443	−2.2
115	0.412	0.401	−2.7

4.2. Diffusion in a 180° turn

The initial conditions for transient diffusion in the 180° turn were assumed to be as follows: the concentration of the running buffer (sodium tetraborate/methanol) was assumed to be one throughout the whole microchannel except for a 50μm length at the inlet (see Fig.1). Here, the analyte (rhodamine B) concentration in that small rectangular zone was set to one, and to zero at all other points in the microchannel.

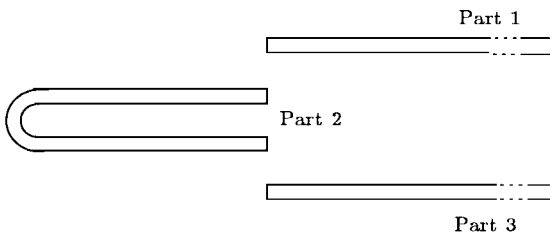


Fig.4. Calculational model of the microchannel with a 180° turn.

In the transient simulation of the 180° turn, we find that the reduction of numerical diffusion is crucial to the solution of the problem. A series of grid sizes has been tried to minimize the impact of numerical errors. As an example, for a coarse grid (~10μm), there is a significant amount of numerical diffusion even as the rhodamine B sample moves through a straight channel. This effect was evaluated by setting the molecular diffusion coefficient to zero. To sufficiently reduce the numerical diffusion, a fine grid of the order of $10^{-6} \sim 10^{-7}$ m in size was used for the final calculations. Additionally, second-order accuracy schemes in both time (second-order, backward) and space (second-order, upwind) were required to sufficiently resolve the time-dependent analyte diffusion. Under these conditions, the numerical diffusion was largely eliminated, showing no significant dispersion when the rhodamine B sample movement was simulated through both a straight channel and the 180° turn channel with the diffusion coefficient set to zero. Additionally, because of computer memory limitations, we divided the experimental channel into three parts: two straight channels and one 180° turn channel (shown in Fig.4) and we solved the three problems separately. The time-dependent outlet conditions of the first problem were used as the inlet boundary conditions of the second problem, while the time-dependent outlet conditions of the second problem were used as the inlet boundary conditions of problem 3. Problems 1 and 3, both for the straight channels, used the same grid geometry containing 305 920 cells, while for the 180° turn (problem 2) the grid geometry having 834 372 cells was used. For the simulation, the first step is to obtain a stable electric potential (shown in Fig.5). Figure 5 shows that the electric field strength varies laterally across the width of the channel in the turn. From the calculated velocity field shown in Fig.6, it can be seen that in the turn, the fluid elements residing at the inner side of the curve flow much faster than those at the outer side of the turn due to the stronger electric field in the former position. Although the velocity field upstream of the curve is relatively flat (which would be expected for a perfectly straight channel), the curve does impact this region, slowing the flow slightly in the centre of the channel. The time sequence shown in Fig.7 follows the analyte as it moves from position A (part 1) to positions B and C (part 2) and then to positions D and E (part 3), traversing the 180°-turn, and highlighting the dispersion. Within the straight channel, the analyte disperses due to diffusion. However, it also disperses significantly within the turn due to the varying velocity profile across the channel width. These simulation results agree well with the five experimental images shown on the right of Fig.7. A more quantitative comparison is presented in Fig.8, where concentration distributions on two segments of the central line are plotted, located normal to marks a and b in Fig.7, respectively. It can be seen that the calculated curves coincide with experimental data. The minor discrepancies between the experiment and simulation could be due to simplifications adopted in the model and a finite experimental data set. As mentioned above, we are using a 2D model, whereas the actual cross section of the channel perpendicular to the flow direction is trapezoidal. This shape might introduce certain three-dimensional effects into the problem which cannot be captured with our existing calculations.

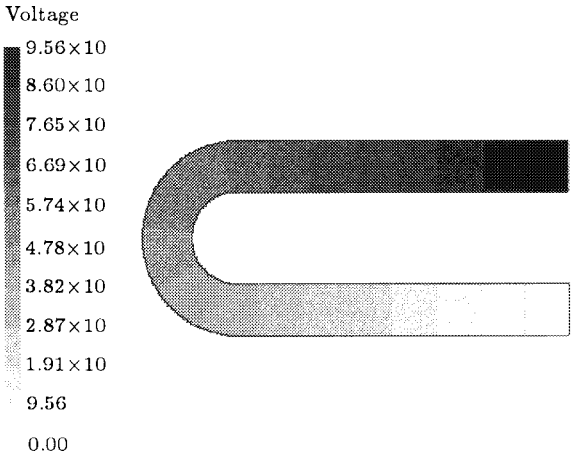


Fig.5. Calculated electric potential field in part 2.

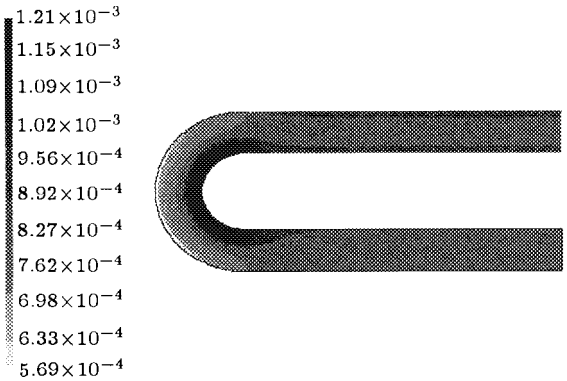


Fig.6. Calculated electro-osmotic velocity field in part 2.

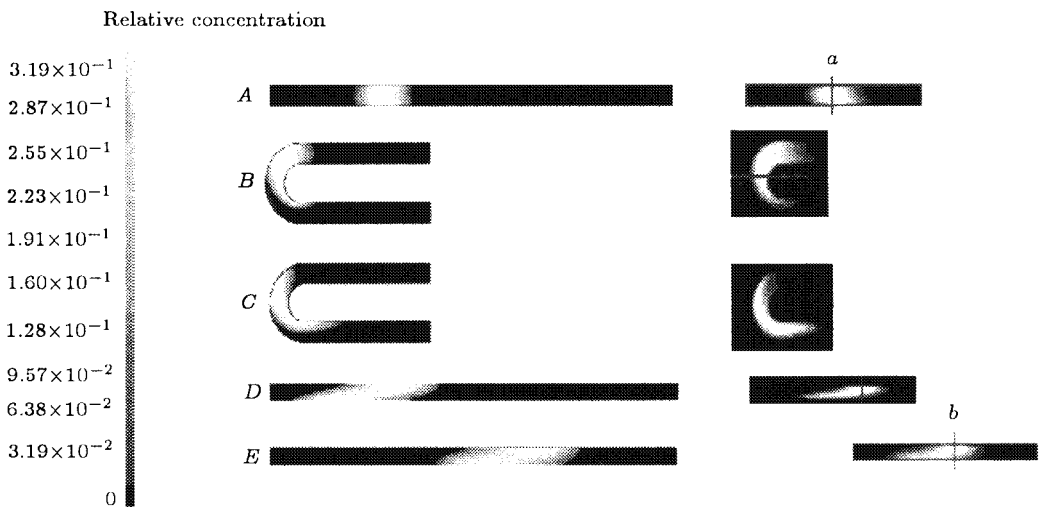


Fig.7. Comparison of calculated (left) and experimental (right) concentration profiles in the 180° turn.

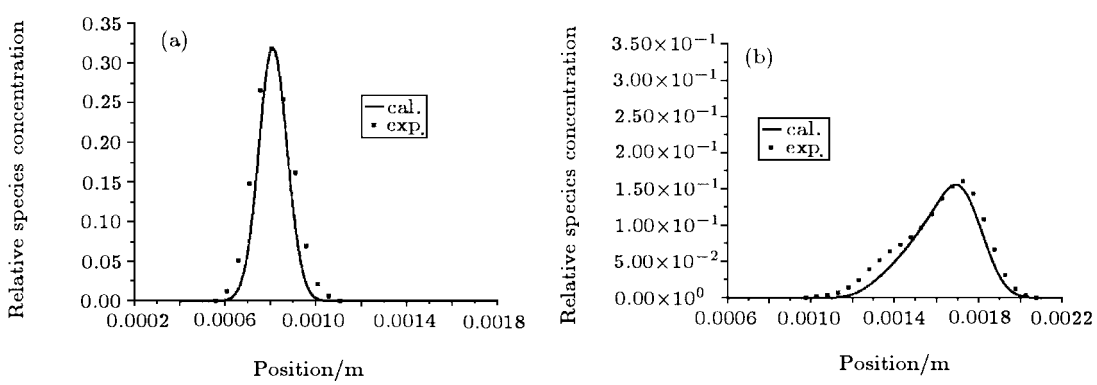


Fig.8. Analytical (cal.) and experimental (exp.) relative species concentration profiles at positions a and b in Fig.7: (a) species concentration distribution at the central line normal to line a in Fig.7; (b) species concentration distribution at the central line normal to line b in Fig.7.

5. Conclusions

We have developed a time-dependent solution scheme for electro-osmotic flow and species transport based on the commercial CFD code, FLUENT. Compared with the experimental results, it has been demonstrated that the improved electro-osmotic force model presented could simulate the electrokinetically driven flow well without calculating the electric charge density distribution within the EDL. Additionally, this model should also be appropriate for applications where pressure gradients exist in the flow field. Using this scheme, we have studied the flow and transport characteristics of an analyte flowing through a microchannel that includes a 180° turn. The detailed structure of the flow field in the microchannel can explain the source of the excessive dispersion introduced by a 180° turn. The introduction of turns adds a geometric contribution to analyte dispersion as both the migration distance and electric field strength vary laterally across the width of the channel in the turns. The results of our simulations agree qualitatively and quantitatively with experimental observation.

Acknowledgment

This research is also sponsored by the Department of Energy Office of Research and Development, USA.

References

[1] Dolnik V, Liu S and Jovanovich S 2000 *Electrophoresis* **21** 41
[2] Jacobson S C and Ramsey J M 1997 *Handbook of Capillary Electrophoresis* ed J P Landers (Boca Raton, FL: CRC Press)
[3] Effenhauser C S 1998 *Topics in Current Chemistry* **194** 51
[4] Effenhauser C S, Bruin G and Paulus A 1997 *Electrophoresis* **18** 2203
[5] Jacobson S C, Hergenroder R, Koutny L B, Warmack R J and Ramsey J M 1994 *Anal. Chem.* **66** 1107
[6] Jacobson S C and Ramsey J M 1995 *Electrophoresis* **16** 481
[7] Culbertson C T, Jacobson S C and Ramsey J M 1998 *Anal. Chem.* **70** 3781
[8] Tian J P and Yao K L 1998 *Acta Phys. Sin.* **47** 1421
[9] Liu M, Chen R, Li H and Kong L 1999 *Acta Phys. Sin.* **48** 1800
[10] Pang X and Li P 2000 *Chin. Phys.* **9** 86
[11] Xiao J, Lu J, Chen J and Li Y 2001 *Chin. Phys. Lett.* **18** 847
[12] Giddings J C 1960 *J. Chromatography* **3** 520
[13] Kasicka V, Prisik Z, Gas B and Stedry C M 1995 *Electrophoresis* **16** 2034
[14] Patankar N A and Hu H H 1998 *Anal. Chem.* **70** 1870
[15] Ermakov S V, Jacobson S C and Ramsey J M 1998 *Anal. Chem.* **70** 4494
[16] Yang C, Li D and Masliyah J H 1998 *Int. J. Heat Mass Transfer* **41** 4229
[17] Jacobson S C and Ramsey J M 1996 *Anal. Chem.* **68** 720
[18] Mosher R A, Saville D A and Thormann W 1992 *The Dynamics of Electrophoresis* (Weinheim: VCH)
[19] Burgeen D and Nakache F R 1964 *J. Phys. Chem.* **68** 1084
[20] Rice C L and Whitehead R 1965 *J. Phys. Chem.* **69** 4017
[21] Hiemenz P C 1986 *Principles of Colloid and Surface Chemistry* (New York: Dekker)